Brain network reorganisation in an adolescent after bilateral perinatal strokes

Large bilateral strokes in adults are often fatal and typically lead to severe functional impairment with little potential for recovery.[1] By contrast, perinatal strokes are associated with variable functional outcomes, with as many as 25% of survivors having healthy motor and cognitive function.[2] Focal cortical injuries sustained in early childhood can be compensated for more quickly and more completely than those sustained later in life.[3] However, the mechanisms underlying cortical plasticity are only beginning to be understood.[4] We have done an exhaustive investigation of one of our patients (PS1; an adolescent male), who sustained large, bilateral perinatal strokes in 1999, but nevertheless had typical neurodevelopment and his injuries went unnoticed until he was 13 years old. The case of this patient underscores the challenge of an accurate prognosis in children after early-life cortical injury.

PS1 was referred to our neurology clinic (St Louis Children's Hospital, MO, USA) in November 2012, because of noted clumsiness of his right hand (video) when he played baseball; he was a left-handed pitcher on a youth baseball team.

PS1's medical history suggested that perinatal strokes occurred 3 weeks postnatally in the setting of dehydration and anaemia after persistent feeding intolerance, vomiting, and diarrhoea, but were not identified at the time (appendix p 2). His subsequent neurodevelopmental trajectory was notable only for a temporary gait asymmetry at 12 months and a persistent, strong left-hand preference. PS1 received speech therapy and reading assistance in early childhood, but attended regular schools throughout adolescence.

Structural MRI revealed extensive bilateral cystic cortical lesions (figure;
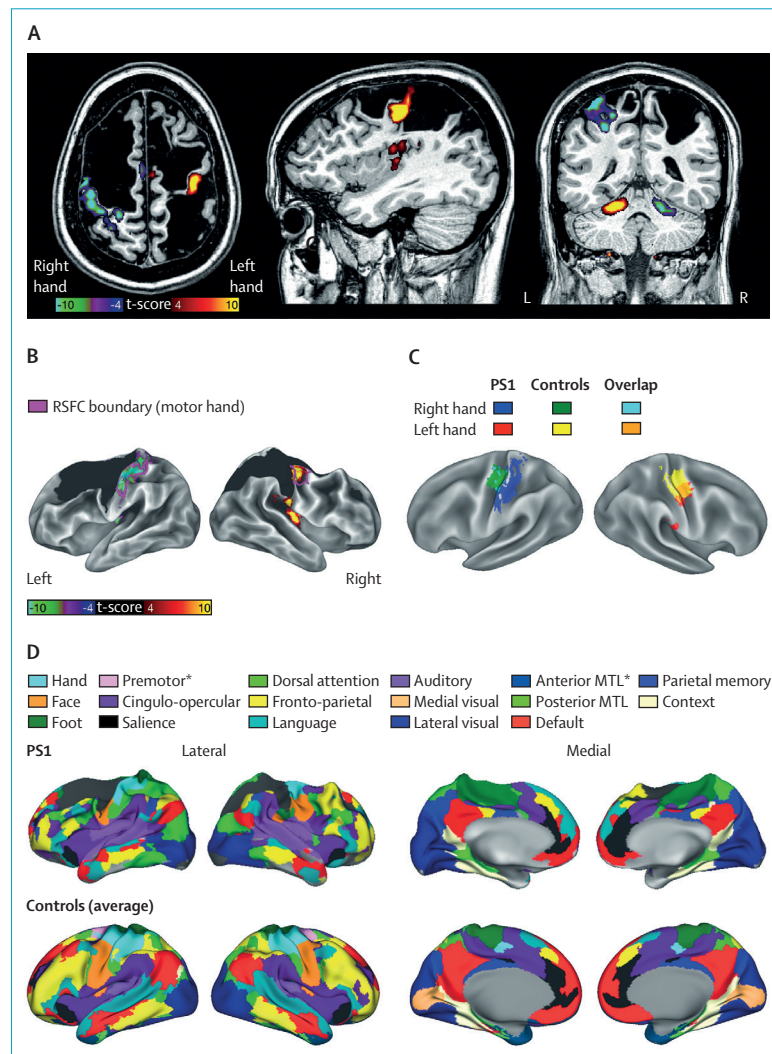

Figure: Functional brain network remapping in PS1 shown by task fMRI and RSFC
(A) fMRI responses to unilateral hand motion (left *vs* right) overlaid on PS1's native space structural MRI that was T1-weighted. Left hand motor fMRI responses (shown in red and yellow) are preserved in intact regions of the motor system, including the spared right hemisphere central sulcus. Right hand motor fMRI responses (green and blue) are displaced to the left hemisphere postcentral gyrus. (B) Hand motor fMRI responses in PS1 overlap with the somatomotor network derived from PS1's RSFC data (magenta outline corresponds with the border of the somatomotor network). The t-score follows the same threshold as in (A). (C) Hand motor fMRI responses in PS1 compared with average location in healthy controls, with a threshold Z-score of 4. Data are projected on an average cortical surface. Left hand activity in PS1 falls nearly entirely within average fMRI response for control of the left hand (orange). Right hand activity in PS1 is completely displaced relative to the average fMRI response for control of the right hand (dark blue). (D) Functional network organisation of PS1 compared with the average of healthy controls. Note the grossly similar topological organisation of the networks (ie, similar spatial adjacency of functional networks). fMRI=functional MRI. MTL=medial temporal lobe. RSFC=resting state functional connectivity. *Networks that were identified in controls but not in PS1.

appendix p 2). This MRI showed that he had lost an estimated 259 cm³, or approximately 20%, of his total supra-tentorial brain volume because of his perinatal injury.

The large disparity between the extent of his brain injury and his functional status justified further investigation. PS1 scored within 2 SD of the mean of age-matched (15 years) standardised scores on intelligence quotient and cognitive function. Motor testing revealed a slight deficit of the right upper limb in strength,

See **Online** for video

See **Online** for appendix

speed, and dexterity relative to the left upper limb (appendix p 7).

Functional MRI (fMRI) has enabled the study of in vivo brain activity in response to tasks. fMRI can also measure patterns of correlated low frequency (<0·01 Hz) activity in resting, awake individuals (resting state functional connectivity [RSFC]).[5] RSFC reveals the brain's functional organisation at the systems level, including, for example, sensory, attention, executive control, language, and memory systems.[6,7] To investigate the remapping of brain function in PS1, we used a newly developed approach to individual-specific precision functional mapping (PFM).[8,9]

PS1 underwent extensive multi-session MRI scans at the East Imaging Building (St Louis, MO, USA) over two summers, beginning when he was aged 15 years (including 285 min of RSFC data and 137 min of task fMRI; appendix pp 3–7). Task fMRI and RSFC data were compared with data from healthy young adults (24–34 years, n=10, 5 female individuals, all right-handed) obtained with the use of the Midnight Scan Club protocol.[9] PS1 also underwent an extensive battery of motor and neurobehavioural assessments at the East Imaging Building, including the National Institutes of Health Toolbox (appendix p 3).

Hand motor tasks showed intact fMRI responses in spared tissue. In the left hemisphere, where the primary motor cortex was nearly completely infarcted, fMRI response showed posterior remapping of function compared with healthy controls (figure A–C; appendix pp 8, 9). PS1's task-based fMRI responses closely aligned with his individual-specific functional network boundaries (figure B). Diffusion tensor imaging showed intact corticospinal tracts arising from both typical (left hand) and displaced (right hand) regions of motor task response (appendix p 10). Finally, RSFC showed a preserved overall organisation of the functional network in intact brain tissue (figure D), with near typical proportions of cortical surface dedicated to each

functional network (appendix p 11). A detailed examination of brain network motifs (ie, the characteristic spatial arrangement of adjacent functional networks) suggested that remapping had occurred primarily in the frontal and parietal association areas (appendix p 12).

Functional network organisation in association areas is incompletely developed at term[10] and shows the greatest interindividual variability in adults.[8] Individual-specific variants in network organisation have been well documented in healthy individuals.[9] However, the number, extent, and pattern of deviations suggest that individual variability alone does not explain our findings in PS1.

Had PS1's infarcts been detected in infancy, his family would probably have been told to expect severe functional impairments. Much to the contrary, PS1 (now aged 22 years) has completed a degree from a technical college and is working in the automotive industry. Future studies that detail the potential for functional remapping relative to tissue loss are needed to provide more accurate prognoses and to understand the factors associated with favourable outcomes, such as those of our remarkable patient.

*Timothy O Laumann, Mario Ortega, Catherine R Hoyt, Nicole A Seider, Abraham Z Snyder, Nico UF Dosenbach, on behalf of the Brain Network Plasticity Group†
laumannt@wustl.edu

†Members and affiliations in the appendix

Department of Neurology (TOL, MO, CRH, NAS, AZS, NUFD), Department of Radiology (AZS, NUFD), Department of Psychiatry (TOL), Department of Biomedical Engineering (NUFD), Department of Pediatrics (NUFD), and Program in Occupational Therapy (CRH, NUFD), Washington University, St Louis, MO 63110, USA

1 Gottesman RF, Sherman PM, Grega MA, et al. Watershed strokes after cardiac surgery: diagnosis, etiology, and outcome. *Stroke* 2006; **37:** 2306–11.

2 Lee J, Croen LA, Lindan C, et al. Predictors of outcome in perinatal arterial stroke: a population-based study. *Ann Neurol* 2005; **58:** 303–08.

3 Benton AL, Tranel D. Historical notes on reorganization of function and neuroplasticity. In: Levin HS, Grafman J, eds. Cerebral reorganization of function after brain damage. New York: Oxford University Press 2000; 3–23.

4 Newbold DJ, Laumann TO, Hoyt CR, et al. Plasticity and spontaneous activity pulses in disused human brain circuits. *Neuron* 2020; **107:** 580–89.e6.

5 Biswal B, Yetkin FZ, Haughton VM, Hyde JS. Functional connectivity in the motor cortex of resting human brain using echo-planar MRI. *Magn Reson Med* 1995; **34:** 537–41.

6 Power JD, Cohen AL, Nelson SM, et al. Functional network organization of the human brain. *Neuron* 2011; **72:** 665–78.

7 Dosenbach NU, Fair DA, Miezin FM, et al. Distinct brain networks for adaptive and stable task control in humans. *Proc Natl Acad Sci USA* 2007; **104:** 11073–78.

8 Laumann TO, Gordon EM, Adeyemo B, et al. Functional system and areal organization of a highly sampled individual human brain. *Neuron* 2015; **87:** 657–70.

9 Gordon EM, Laumann TO, Gilmore AW, et al. Precision functional mapping of individual human brains. *Neuron* 2017; **95:** 791–807.e7.

10 Smyser CD, Inder TE, Shimony JS, et al. Longitudinal analysis of neural network development in preterm infants. *Cereb Cortex* 2010; **20:** 2852–62.

Inspiring the next generation

The Neurology and Neurosurgery Interest Group (NANSIG) has been organising career conferences for health professionals in training in the UK and Ireland since 2011. NANSIG has become a trusted source of information for trainees across the world, as we have a wealth of feedback from past attendees to guide our events. Our tenth annual conference (held online on Jan 30, 2021) attracted 227 delegates from 26 countries, which was substantially more people than attended previous conferences in person (ie, 79–123 delegates in 2018–20). This event was held virtually due to the COVID-19 pandemic, which regrettably reduced opportunities for personal interaction and hands-on demonstration but fortunately increased accessibility; reduced logistical costs, allowing a free event; and facilitated international participation.

THE LANCET
Neurology

Supplementary appendix

This appendix formed part of the original submission. We post it as supplied by the authors.

Appendix

Brain Network Reorganisation in an Adolescent After Bilateral Perinatal Strokes

Timothy O. Laumann, Mario Ortega, Catherine R. Hoyt, Nicole A. Seider, Joshua S. Siegel, Annie L. Nguyen, Donna L. Dierker, Rebecca S. Coalson, Babatunde Adeyemo, Scott Marek, Adrian W. Gilmore, Steven M. Nelson, Joshua S. Shimony, Deanna J. Greene, Marcus E. Raichle, Evan M. Gordon, Steven E. Petersen, Bradley L. Schlaggar, Abraham Z. Snyder, Nico U.F. Dosenbach

Departments of Neurology (TOL, MO, CRH, NAS, SM, ALN, RSC, BA, MER, SEP, AZS, NUFD), Radiology (DLD, RSC, JSS, DJG, MER, SEP, AZS, NUFD), Psychiatry (TOL, JSS, SM, DJG), Neuroscience (JSS, MER, SEP), Biomedical Engineering (MER, SEP, NUFD), Psychological and Brain Sciences (AWG, SEP), Pediatrics (NUFD), Program in Occupational Therapy (CRH, NUFD) – Washington University in St. Louis

VISN 17 Center of Excellence for Research on Returning War Veterans (SMN, EMG)

Center for Vital Longevity, School of Behavioral and Brain Sciences, Department of Psychology and Neuroscience – University of Texas at Dallas (SMN, EMG)

Kennedy Krieger Institute (BLS)
Department of Neurology, Department of Pediatrics (BLS) – Johns Hopkins University

† All authors belong to the Brain Network Plasticity Group (TOL, MO, CRH, NAS, JSS, ALN, DLD, RSC, BA, SM, AWG, SMN, JSS, DJG, MER, EMG, SEP, BLS, AZS, NUFD)

Table of Contents
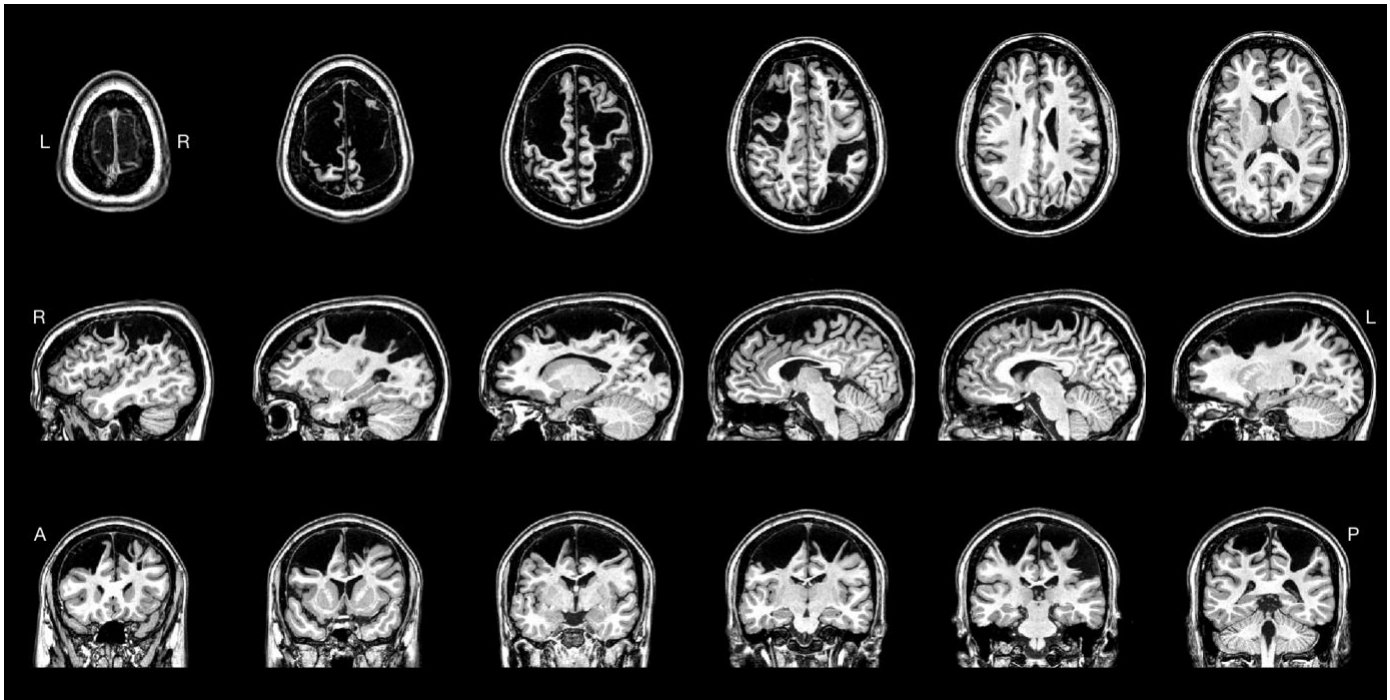
Clinical History

Figure S1. PS1's T1-weighted structural MRI (0.8 mm) demonstrates extensive bilateral tissue loss in frontal and parietal cortex.

PS1, a left-handed, 13-year-old male who played for a competitive youth baseball team, was referred to an orthopedic physician for evaluation of his right arm. While being able to throw from outfield to home with his left arm, he had difficulty using his right arm effectively (see Video S1 for example of PS1's motor function). Ulnar neuropathy was considered and he was referred for physical therapy. However, PS1 was first seen by a child neurologist (NUFD) for further evaluation. Structural brain MRI revealed unexpectedly extensive bilateral cystic lesions consistent with perinatal infarcts (Figure S1; [1]).

Review of PS1's medical history revealed that the injury occurred in the perinatal period. Patient PS1 was born at 36 weeks following an uncomplicated pregnancy. He was reportedly doing well until day of life 6 when he had a brief apneic event (15-20 seconds) and was evaluated in the emergency department but not hospitalized. Between day of life 6 and 18 he developed poor feeding, vomiting, and diarrhea, leading to persistent lethargy. On day of life 18, he was admitted to the ICU, where he was found to be dehydrated, hypothermic (93.7°F), acidotic (pH 6.9), and anemic (hematocrit 20). He received IV fluids and blood transfusion. On day of life 20, his neurologic exam was reported as non-focal. Brain imaging was obtained on day of life 21. Head CT was reported to show "patchy hypodensity" in posterior temporal, parietal, and occipital areas. However, MRI (including diffusion-weighted imaging) on the same day was reported as normal. Extensive work-up of diarrhea and feeding intolerance was ultimately unrevealing. Following recovery, subsequent neurodevelopmental trajectory was notable only for a temporary gait asymmetry at 12 months and a persistent, strong left-hand preference. PS1 received early childhood assistance in speech and reading, but otherwise typical schooling through adolescence. PS1 opted for vocational high school. His mother works as a paralegal and his father as an HVAC technician.

Background

The prognosis following perinatal stroke is variable, but, in general, more favorable than in adults. Death is uncommon [2] although motor or neurocognitive deficits occur at rates variably estimated as between ~40% and ~75% [2-7]. Thus, a substantial fraction of long-term survivors of perinatal stroke either develop typically or with only slight delays and/or impairments.

It is widely thought that functional remapping underlies recovery of function following stroke, in adults as well as infants [8-12]. Much of the evidence supporting this perspective has been obtained by neuroimaging studies

demonstrating aberrant functional responses in intact parts of the brain not normally recruited by task functional MRI (fMRI) paradigms [9, 13-15]. Parallel findings have more recently been obtained by resting state (i.e., task-free) fMRI [16-19]. The markedly better prognosis following neonatal as opposed to adult stroke is widely understood as reflecting enhanced neuroplasticity early in life [8]. The earliest indications of enhanced neuroplasticity early in life were obtained by lesion experiments in monkeys [20]. This perspective has acquired nuance in the light of more recent data [3, 21, 22] but remains essentially valid. Studies in school age children suggest that the period of heightened neuroplasticity is largely over by the age of 3 years [23].

Thus, it is clear that the relatively favorable prognosis following neonatal stroke reflects functional remapping at a developmental stage when this is most possible. However, this understanding derives largely from the study of neonatal arterial ischemic stroke (AIS), hence, unilateral lesions, in which function is subsequently remapped to homotopic parts of the intact hemisphere, e.g., [19]. Here, we describe a patient (PS1) who sustained a hypotensive event at the age of ~3 weeks leading to a watershed stroke involving both hemispheres. This case is remarkable also because of the marked discrepancy between the patient's functional status in relation to the extent of the infarcts.

Methods

PS1 underwent extensive, multi-session MR imaging (including 285 minutes of resting-state fMRI data) using the Midnight Scan Club (MSC) protocol, a study of brain organization in young adults (24-34 years old, n = 10, 5 female, all right-handed; [24]). All subjects were scanned at Washington University in St. Louis, using a Siemens TIM TRIO scanner equipped with a 12-channel head coil. All protocols for T1-weighted, T2-weighted and fMRI scans were identical across individuals. Data acquisition and analysis were performed with the approval of the Washington University Institutional Review Board. Written informed consent was provided by PS1's mother and assent was given by PS1 at the time of data acquisition. Written consent by PS1's mother and PS1's assent was also obtained for use of video images of PS1.

Neuropsychological Evaluation

PS1 completed a cognitive assessment including the Kaufman Brief Intelligence Test-2 (KBIT) [25] and the cognitive battery from the National Institute of Health (NIH) toolbox [26]. The KBIT measures verbal and nonverbal intelligence; a composite score below 85 indicates below-average intelligence, and a score below 70 indicates intellectual disability. The NIH toolbox assesses broader concepts linked to functional cognition, including language, attention, working and episodic memory, executive function, and processing speed. Assessment included Picture Vocabulary, Flanker Inhibitory Control and Attention Test, Picture Sequence Memory Test, List Sorting Working Memory Test, Dimensional Change Card, Pattern Comparison Processing, and Oral Reading Recognition. Details of these tests can be found at www.nihtoolbox.org. Additional psychiatric and behavioral assessments included the Child Behavior Checklist (CBCL) [27], Child Depression Inventory (CDI-2) [28], and Connors ADHD screen (3rd edition) [29], which did not identify any clinical significant concerns in PS1.

Motor Assessments

PS1 was screened for general motor function impairment using the Abilhand for kids [30] and Movement Assessment Battery Checklist for Children [31], which indicated modest but clinically significant motor impairment (Abilhand indicated difficulty with 7 out of 21 ADLs; Movement in Static/Predictable Environment Score: 12 Movement in Dynamic or Unpredictable Environment Score: 5). Detailed hand motor function was evaluated using several standard tests of motor strength, speed, fluency and dexterity. All measures were administered by an occupational therapist (CHD) over several in-person visits. Grip strength was measured with a Jamar Smart Hand Digital Dynamometer (Patterson Medical, Warrenville). PS1 was instructed to form a closed fist around a handle on the dynamometer, keeping the arm at the side with the elbow bent at 90°, and squeeze as tightly as possible. Pinch strength was assessed using a Jamar Hydraulic Pinch Gauge (Patterson Medical, Warrenville). Maximal force was recorded in pounds. Finger-tapping speed was measured in 10-second increments using an electronic tapping test (WPS, Torrance, CA). Mean values for grip strength, pinch strength, and finger-tapping were computed across 3 trials at 2 separate visits.

Gross upper extremity dexterity and coordination was evaluated using the Box and Blocks Test. For this test, individuals are instructed to pick up blocks one at a time and move as many as possible from one side to the other over a barrier in one minute. It is widely used across disciplines and clinical populations because of the ease of administration and objective outcomes. Scores were averaged from two separate visits.

PS1's grip strength, pinch strength, finger-tapping, and Box and Blocks score were compared to extant normative references matched for age at time of administration (15 years old) and gender (male): grip and pinch strength from [32]; finger-tapping from [33]; and Box and Blocks score from [34]. PS1's left hand is his dominant hand and his right hand is his non-dominant hand. For reference datasets in which data were not explicitly sorted by hand dominance, reported subject characteristics suggested that right hand values could be treated as the dominant hand, while left hand values could be treated as the non-dominant hand. A reference comparison 'Z-score' was computed as: (<PS1 value> - <ref mean value>) / <ref SD value>.

Further assessment of range of motion, accuracy, fluency of movement, and dexterity of PS1's non-dominant limb was performed using the Melbourne Assessment 2 (MA2). The Melbourne Assessment is a 14-item motor assessment for children ages 2.5 to 15 with either a congenital or acquired neurological condition [35].

MR Image Acquisition

For MSC subjects, data were acquired as described in previous work [24]. Briefly, structural MRI was acquired across two separate days including four T1-weighted images (sagittal, 224 slices, 0.8 mm isotropic resolution, TE=3.74 ms, TR=2400 ms, TI=1000 ms, flip angle = 8 degrees), and four T2-weighted images (sagittal, 224 slices, 0.8 mm isotropic resolution, TE=479 ms, TR=3200 ms). Functional MRI data were collected across 10 additional sessions. Resting state fMRI data were collected in 30-minute contiguous runs in each session (300 minutes total per subject). Each session also included one hour of task fMRI data including three tasks, only the motor task (described below) is relevant here. All functional imaging was performed using a gradient-echo EPI sequence (TR = 2.2 s, TE = 27 ms, flip angle = 90°, voxel size = 4 mm x 4 mm x 4 mm, 36 slices). For each session, one gradient echo field map sequence was acquired with the identical lattice size as the functional scans.

PS1's image acquisition parameters were identical to those of the MSC cohort with a few exceptions. Five T1-weighted and four T2-weighted scans were averaged together to obtain high resolution structural images of PS1. In order to maximize comfort and tolerance, resting state fMRI runs for PS1 were limited to only 8 contiguous minutes. Two or three runs were collected on each of 17 sessions (285 minutes total).

Functional MRI Motor Task Design

The motor task was adapted from the Human Connectome Project (HCP) [36]. Subjects were instructed to close and relax their hands, flex and relax their toes, or wiggle their tongue based on a visual cue. Each block of the task began with 2.2 s cue indicating which movement was to be made. A centrally presented caret replaced the instruction and flickered once every 1.1 s (without temporal jittering) to indicate that the subject should execute the proper movement. 12 movements were made per block. Each task run consisted of 2 blocks of each type of movement, as well as 3 blocks of resting fixation lasting 15.4 seconds. Fifteen of PS1's functional imaging sessions included between 2-4 runs of this task (36 runs total; 137 minutes total). MSC subjects performed 2 runs of the motor task across 10 sessions (76 minutes total).

Diffusion Tensor Imaging (DTI)

Diffusion tensor imaging (DTI) was acquired on PS1 and MSC02 in order to measure white matter tracts. Single-shot echo planar diffusion-weighted MRI data were acquired on a Siemens 3T Trio using a 12-channel head coil. Sequence parameters were as follows: 80 contiguous axial slices, isotropic ($2\times2\times2$ mm^3) resolution, and pulse repetition time/echo time 14500/94 ms. During each scanning session, 45 diffusion-weighted images (maximum b-value of $1.4*10^3$ s/mm^2) and 6 B0s were acquired, for a total of 51 volumes. For PS1, seven such diffusion weighted scans were obtained, for a total of 357 diffusion-weighted images. For MSC02, 15 such diffusion weighted scans were obtained, for a total of 765 diffusion weighted images. Eddy correction was applied to each scan [37]. Diffusion-weighted images were registered to each other and concatenated into a single 4D matrix. The Diffusion Tensor Image was calculated from all DWI using a non-negative least squares calculation. We then used a deterministic approach for tract creation, following the National Alliance Medical Imaging Center (NA-MIC) protocol [38]. The regions of interest (ROI) to initiate tractography were defined from

the motor task maps for left and right hand fMRI responses thresholded at Z = 2.96. The fibers traced from the original starting ROI are then sub-selected as intersecting the pyramids.

Cortical Surface Generation

PS1's cortical surface was generated following a procedure similar to that previously described in [39] and [40] for the MSC subjects. First, five T1-weighted scans were registered and averaged together to reduce noise. This average T1-weighted image was passed through FreeSurfer's default recon-all pipeline (version 5.3) in native volumetric space. This pipeline performs brain extraction (i.e., skull stripping) and segmentation. The segmented volume was then carefully hand-edited to distinguish stroke-related voxels from gray and white matter. Within the FreeSurfer pipeline, special considerations were taken to create accurate surface contours for subject PS1 as follows: 1) manual edits to the surface points were added to capture the isolated left hemisphere and right hemisphere motor gyri "tendrils" that were under-represented in first-pass default processing pathways. 2) White matter (WM) control points were also added to these regions to demarcate the low-WM signals seen in these areas.

The hand-edited segmentation was then passed through the remainder of the recon-all pipeline, which generates white matter and pial surfaces, inflates the surfaces to a sphere, and performs surface shape-based spherical registration to the fsaverage surface [41, 42]. The fsaverage left and right hemisphere surfaces have previously been brought into register with each other using deformation maps from a landmark-based registration of left and right fsaverage surfaces to a hybrid left-right fsaverage surface ('fs_LR'; [43]). PS1's surfaces were registered to the atlas using a flexible Multi-modal Surface Matching (MSM) algorithm [44]. Cortical sulcal depth maps, excluding areas falling within the hand-edited surface lesion masks, were used to achieve alignment between the individual and the fs_LR atlas. The registered surfaces were then down-sampled to a 32,492 vertex surface (fs_LR 32k) for each hemisphere. The deformations from the original surfaces to the fs_LR 32k surface were composed into a single deformation map allowing for one step resampling. Surfaces in native stereotaxic space were then transformed into atlas space (711-2B) by applying the previously calculated T1-to-atlas transformation.

Due to the unique morphology of PS1's stroke, an expert rater (MO) consulted with a neuroradiologist (JSS) to confirm the edge boundaries of PS1's infarct. The final stroke surface was verified (and edited where necessary) in areas that had confirmed infarcted tissue. Boundary areas of the stroke were delineated manually with the aid of additional corroborating brain measures including cortical thickness, BOLD signal-to-noise ratio (SNR), and cortical myelin maps [45].

fMRI Preprocessing

Functional data from PS1 and the MSC dataset were preprocessed identically following previously described procedures to reduce artifact and to maximize cross-session registration [24]. All sessions underwent correction of odd versus even slice intensity differences attributable to interleaved acquisition, intensity normalization to a whole brain mode value of 1000, and within run correction for head movement. Atlas transformation was computed by registering the mean intensity image from a single BOLD session to Talairach atlas space [46] via the average high-resolution T2-weighted image and average high-resolution T1-weighted image. All subsequent BOLD sessions were linearly registered to this first session. This atlas transformation, mean field distortion correction (see below), and resampling to 3-mm isotropic atlas space were combined into a single interpolation using FSL's applywarp tool [47]. Subsequent operations were performed on the atlas-transformed volumetric time series.

fMRI Distortion Correction

A mean field map was generated based on the field maps collected from each session on PS1 and the MSC control subjects following a procedure previously described in [39]. This mean field map was then applied to all sessions for distortion correction in a given subject. To generate the mean field map the following procedure was used: (1) Field map magnitude images were mutually co-registered. (2) Transforms between all sessions were resolved. Transform resolution reconstructs the n-1 transforms between all images using the n*(n-1)/2 computed transform pairs. (3) The resolved transforms were applied to generate a mean magnitude image. (4) The mean magnitude image was registered to an atlas representative template. (5) Individual session magnitude image to atlas space transforms were computed by composing the session-to-mean and mean-to-

atlas transforms. (6) Phase images were then transformed to atlas space using the composed transforms, and a mean phase image in atlas space was computed.

Application of mean field map to individual fMRI sessions: (1) For each session, field map uncorrected data was registered to atlas space, as above. (2) The generated transformation matrix was then inverted and applied to the mean field map to bring the mean field map into the session space. (3) The mean field map was used to correct distortion in each native-space run of resting state and task data in the session. (4) The undistorted data was then re-registered to atlas space. (5) This new transformation matrix and the mean field map then were applied together to resample each run of resting state and task data in the session to undistorted atlas space in a single step.

fMRI Task Analyses

Task evoked activations were modeled individually for each voxel with a general linear model (GLM) [48], using in-house image analysis software written in IDL (Research Systems, Inc.). First level analyses were conducted separately for each session in a given subject, and second level analyses grouped data across the ten (or 15, in the case of PS1) sessions of a single subject. We computed voxelwise t-tests on task response contrasts between left versus right hand, left versus right foot, and tongue versus bilateral hands and feet. Comparisons to the group average results were made in atlas space. PS1 specific responses were visualized following transform back into native subject space. Task responses were also sampled on to the cortical surfaces for visualization.

Resting State Functional Connectivity (RSFC) Preprocessing

Prior to computing resting state functional connectivity (RSFC), a number of additional preprocessing steps were performed to reduce spurious variance related to motion and physiologic artifacts [49, 50]. Temporal masks were created to flag motion-contaminated frames. Two of the MSC subjects (MSC03 and MSC10) had a high-frequency artifact in the motion estimates calculated in the phase encode (anterior-posterior) direction that did not appear to reflect biological movement [51, 52]. Motion estimate time courses in these subjects in this direction were low-pass filtered to retain effects occurring below 0.1 Hz (see [51, 52] for further discussion of this phenomenon). Motion contaminated volumes were identified by frame-by-frame displacement (FD; [53]). Frames with FD > 0.2 mm were flagged as motion-contaminated. Across all MSC data, temporal masks retained 72% ± 18% of frames. In PS1, temporal masks retained 79% ± 14% of frames.

After computing the temporal masks for high motion frame censoring, the data were processed with the following steps: (i) demeaning and detrending, (ii) linear interpolation of censored frames to enable (iii) band-pass filtering (0.005 Hz < f < 0.01 Hz) without re-introducing nuisance signals [54] or contaminating frames near high motion frames [53, 55] and; (iv) regression of multiple nuisance waveforms derived from the whole brain, motion regressors, and ventricular, white matter, and extra-axial signals. The nuisance waveforms were obtained using a CompCor-like [56] dimensionality reduction procedure described in detail in [57]. Censored frames were excised from the data for all subsequent analyses.

Sampling Volume Data to the Surface

Functional MRI (BOLD) volumetric timeseries were sampled to each subject's cortical surface using previously described procedures [24, 39]. In brief, data were sampled to the 'mid-thickness' surface (average position between pial and white surfaces) using the 'ribbon-constrained' sampling function in Connectome Workbench. This procedure samples from voxels in the gray matter ribbon that lie in a cylinder orthogonal to the local mid-thickness surface weighted by the extent to which the voxel falls within the ribbon [45]. To reduce the effect of large blood vessels near the cortical surface, voxels with a timeseries coefficient of variation 0.5 standard deviations higher than the mean coefficient of variation of nearby voxels (within a 5 mm neighborhood) were excluded during the volume to surface sampling [58]. Data were then resampled from the individual's original surface to the 32k fs_LR surface in a single step. This resampling allows point-to-point comparison between each individual registered to the 32k_fs_LR space.

Functional Network Mapping

The network organization of the MSC subjects and PS1 were derived using the graph-theory-based Infomap algorithm for community detection [59], following [60]. The MSC average resting state network organization

has been previously published in [24]. The same procedure was followed for finding networks in PS1 with slight modification to account for the infarct. In brief, for this procedure, the Pearson correlation matrix of the time courses from all cortical vertices for each session is computed and then averaged across sessions. For PS1, infarcted portions of the cortical surface (based on the hand-edited surface lesion masks) were removed from this matrix. Correlations between vertices closer than 30 mm (geodesic distance) were set to zero to compensate for spatial smoothing performed during sampling of voxel value surface vertices. Geodesic distance was used for within-hemisphere surface connections. Inter-hemispheric connections between the cortical surfaces were retained, as smoothing was not performed across the mid-sagittal plane. The correlation matrix was then thresholded at multiple thresholds to achieve edge densities in the range of 0.1% to 5%. These thresholded matrices were used as inputs for the Infomap algorithm, which calculated community assignments (representing brain networks) separately for each threshold. Small communities with 400 or fewer gray-ordinates were considered unassigned and removed from further consideration. Regions smaller than 10 vertices were also removed and recolored by adjacent networks.

Putative network identities were then assigned following a consensus procedure described in [24]. First, communities at each threshold were matched to a set of networks identified in data averaged across a large independent group of healthy adults [39]. This matching approach proceeded as follows. At each density threshold, all identified communities in PS1 were compared using spatial overlap (quantified by Jaccard index) to each one of the group networks in turn. The best-matching (highest-overlap) community was assigned that network identity; that community was not considered for comparison with other networks within that threshold. If the Jaccard index was below 0.1, the network would be left 'unidentified'. Matches were first made with the large, well-known networks (e.g., Default, Lateral Visual, Motor, Cingulo-Opercular, Fronto-Parietal, Dorsal Attention, Language), and then to the smaller, less well-known networks (e.g., Salience, Parietal Memory, Context Association, Motor Foot). The average Jaccard value for PS1 networks corresponding to the group average template was 0.36 (range 0.12-0.53). A "consensus" network assignment was then derived by collapsing assignments across thresholds, giving each node the assignment it had at the sparsest possible threshold at which it was successfully assigned to one of the known group networks. The assignments from PS1 were closely examined to ensure that the exclusion of the infarcted vertices did not affect the quality of this matching procedure.

Resting State Network Topography

Functional connectivity maps representing resting state network topography for a given network were computed by averaging the correlation maps from all vertices identified by Infomap as belonging to that network (See Figure S7).

Role of Funding Sources

The funding sources had no direct role in the design, collection, or analysis of the data herein.

A) Neuropsychological Tests

Kaufman Brief Intelligence Test	Score
IQ (standardized composite)	**85**
Verbal intelligence	92
Non-verbal intelligence	82

NIH Toolbox Scores (standardized)	Score
Picture sequence memory	106.5
List sorting working memory	95.4
Oral reading recognition	81.6
Flanker Inhibitory task	76.6
Picture Vocabulary task	95.3
Dimensional change card sort task	77.4
Pattern comparison processing speed	75.2

B) Motor Tests

Hand function	Left	Right
Grip strength lbs. [Z-score]	79.7 [0.2]	45.3 [-1.3]
Pinch strength lbs.	23.6 [0.7]	16.2 [-1.0]
Fingertaps (per 10-sec)	56.0 [-1.1]	27.7 [-6.1]
Box & Blocks score (#)	47.5 [-3.4]	37.0 [-4.8]

Table S1. A) Neuropsychological testing demonstrated PS1's cognitive function was within normal range. Reported values are age-adjusted standardized scores (Mean = 100, SD = 15) from the NIH Cognition Toolbox Battery. B) Motor evaluation demonstrated PS1's mild paresis of the right hand on tests of strength and dexterity. The left hand was mostly within normal range, with a modest deficit in dexterity. The bracketed values reflect the Z-score relative to age and gender-matched reference ranges for each test.

Results

PS1 Suffered Extensive Symmetrical Perinatal Strokes

The extent of PS1's infarcts is illustrated in Figure S1. The left hemisphere sustained extensive loss of frontal cortex, including near total loss of the central sulcus and pre-central gyrus, as well as losses in middle and superior frontal gyri. Cortical loss on the right was even more extensive and involved both frontal and parietal cortex, but with notable sparing of inferior pre- and post-central gyri. PS1 lost approximately 259 cubic centimeters or ~20% of total supratentorial brain volume (average male control subject: 1186 cm^3; PS1: 972 cm^3). This injury is presumed to be consequent to strokes that occurred around 18-21 days postnatally. Despite this injury, PS1 developed with typical cognitive abilities and near typical motor abilities (Table S1A). Motor testing revealed a deficit in the right upper limb in strength, speed, and dexterity relative to the left upper limb (Table S1B).
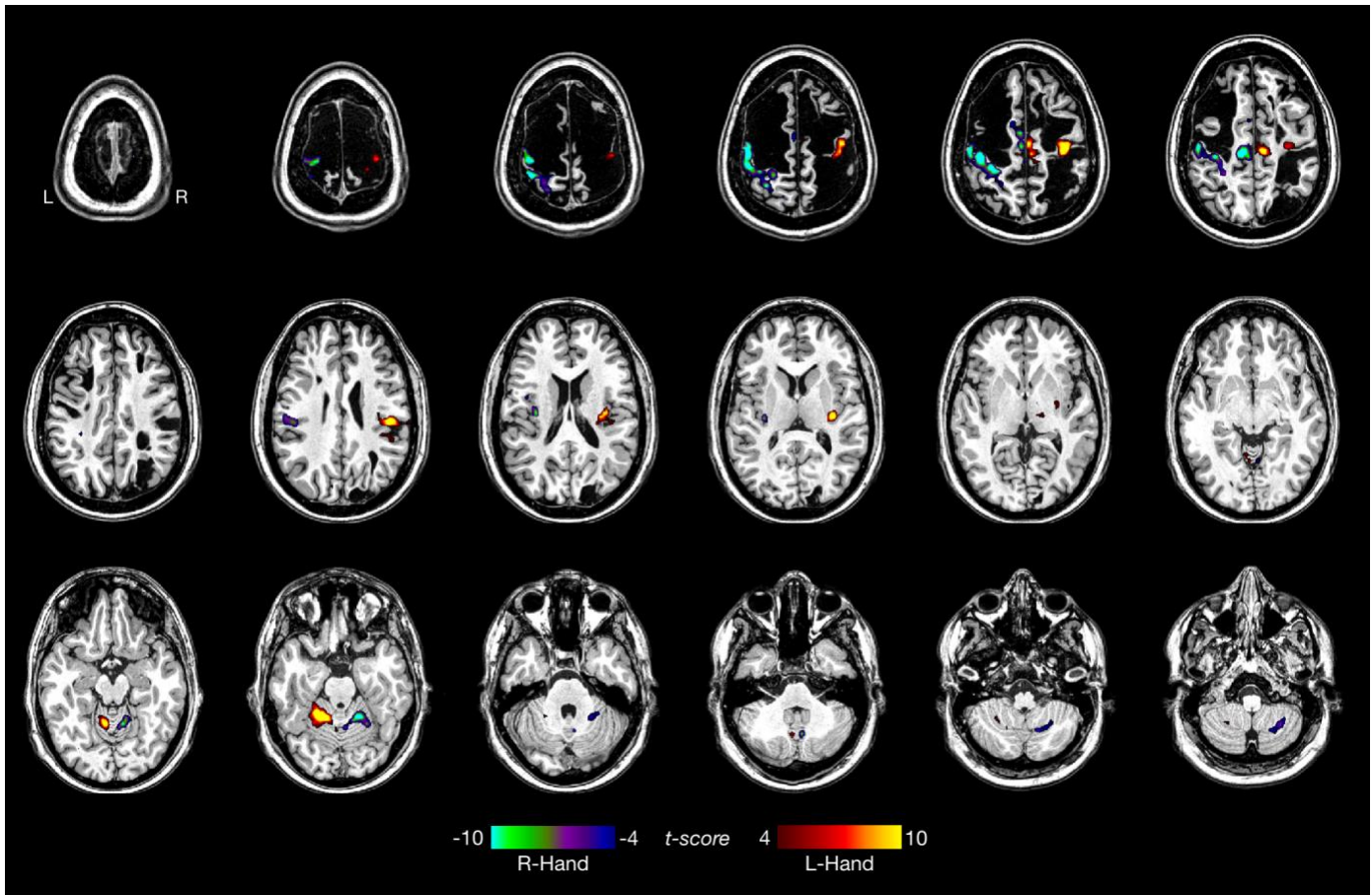
Figure S2. Functional MRI (fMRI) responses to unilateral hand motion in PS1 (left versus right).

Task and Resting-State fMRI of Motor Representation

PS1's fMRI responses to hand movements exhibited archetypal mapping in subcortical (putamen and thalamus) and cerebellar regions (including multiple discrete representations; Figure S2; [40]). In the cortex, right hand motor task responses activated the post-central gyrus of the left hemisphere, demonstrating posterior remapping of motor function. Left hand motor task responses were intact, but restricted to a remarkably small, preserved portion of inferior right hemisphere motor cortex. PS1's left hand motor representation fell entirely within the average location of motor task response seen in typical controls (Figure 1B, orange), while PS1's right hand motor representation shows almost no overlap (Figure 1B, dark blue). These observations potentially account for PS1's left hand dominance and mild right hemiparesis. PS1's idiosyncratic representation of motor function was mirrored in the organization of his functional networks as measured with RSFC (Figure 1C).
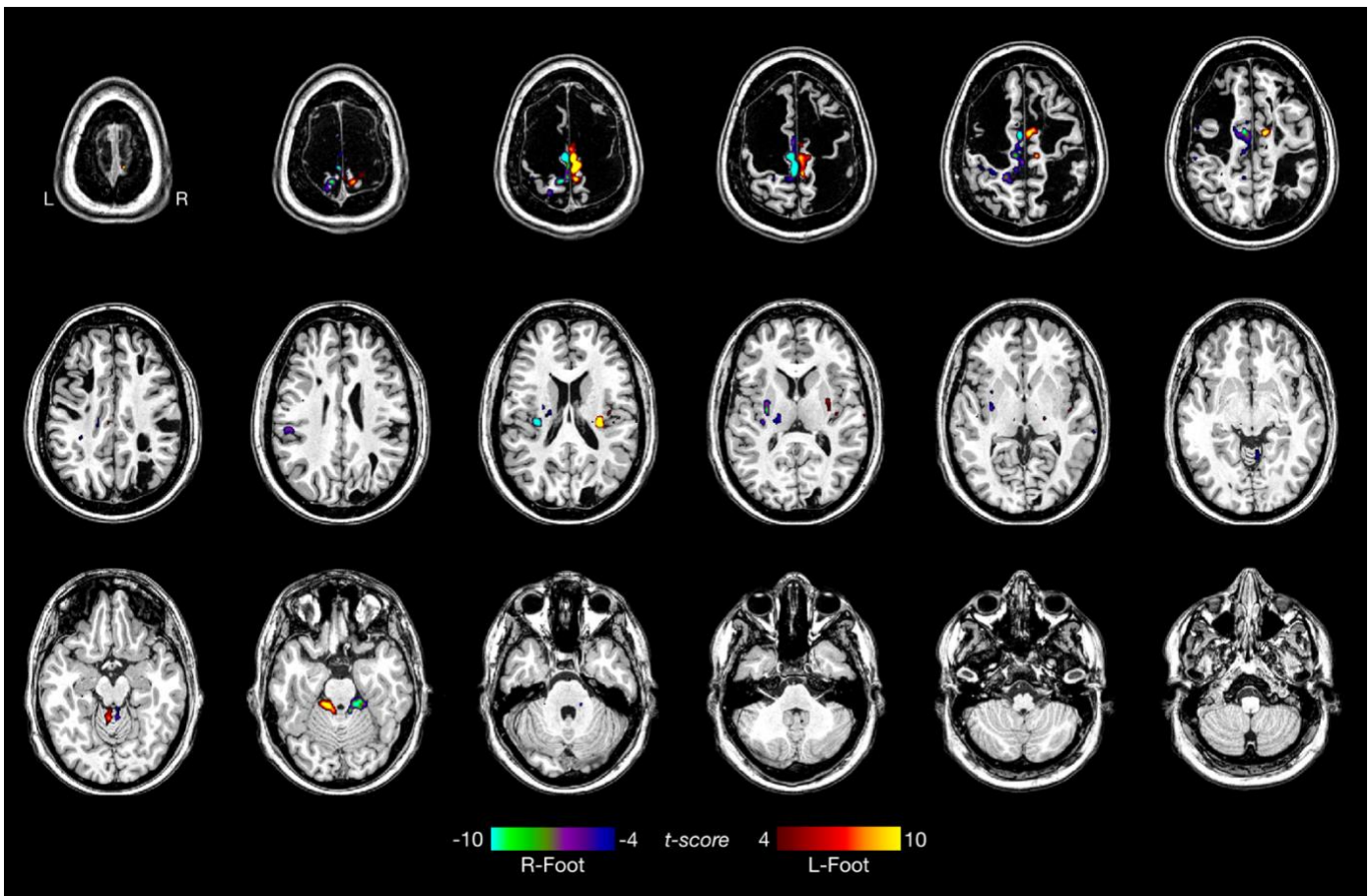
Figure S3. Functional MRI (fMRI) responses to unilateral foot motion in PS1 (left versus right).
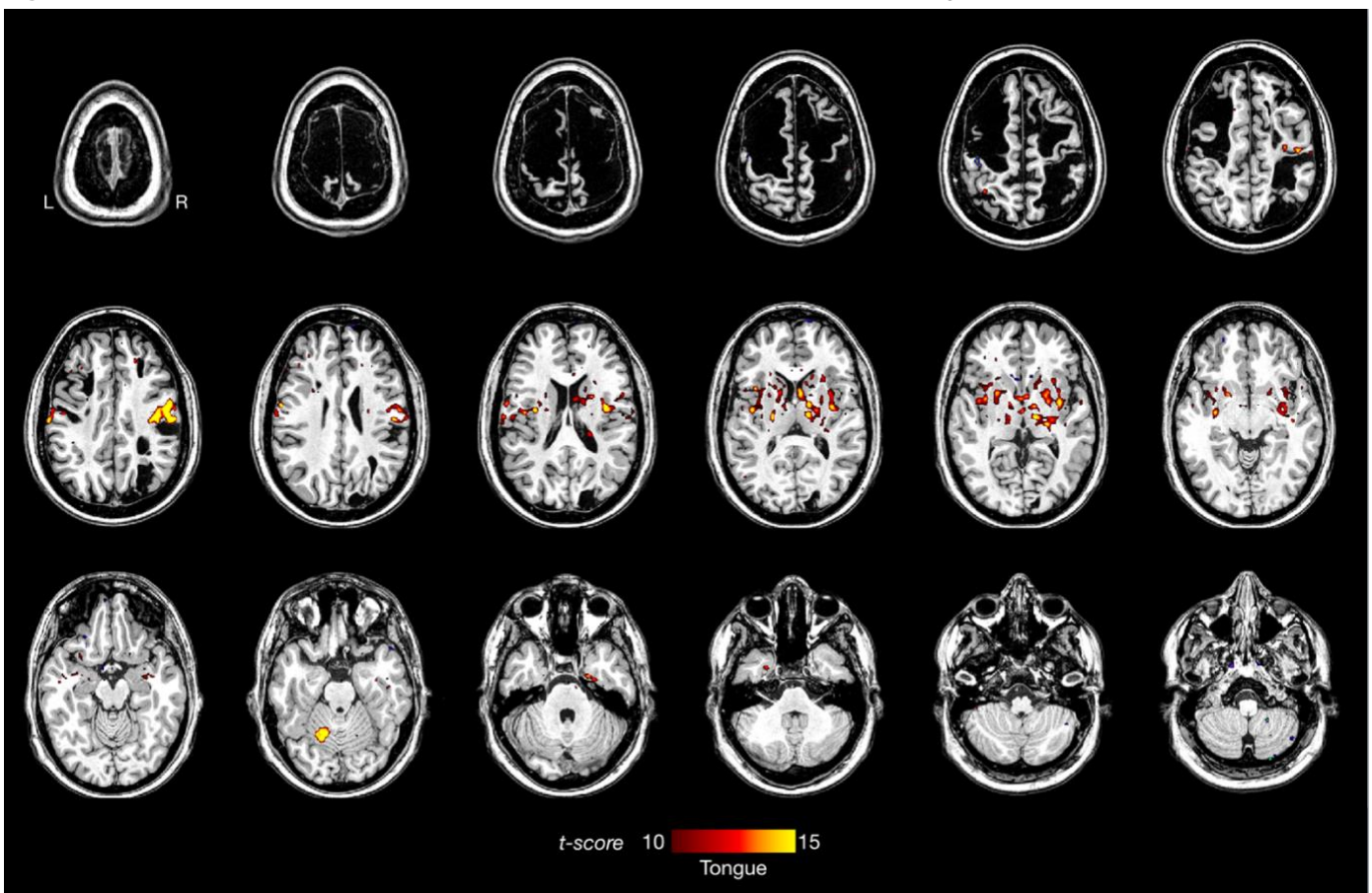

Figure S4. Functional MRI (fMRI) responses to tongue motion in PS1 (tongue versus bilateral hands and feet).

Foot movements exhibited archetypal somatotopic organization with activation along the dorsal medial parietal cortex, bilateral insula, and bilateral cerebellum (Figure S3). Similarly, the tongue movements exhibited somatotopic localization with activation along the ventral lateral aspect of the central sulcus (Figure S4). Notably, tongue movement activations were significantly noisier than the hand and foot movements - a phenomenon previously observed, likely related to the effect of tongue movements on magnetic susceptibility in the head. This excess noisiness warranted higher statistical thresholds to highlight meaningful activations (note elevated t-statistic threshold (t>10) for this contrast relative to the hand and foot contrasts (t>4)).
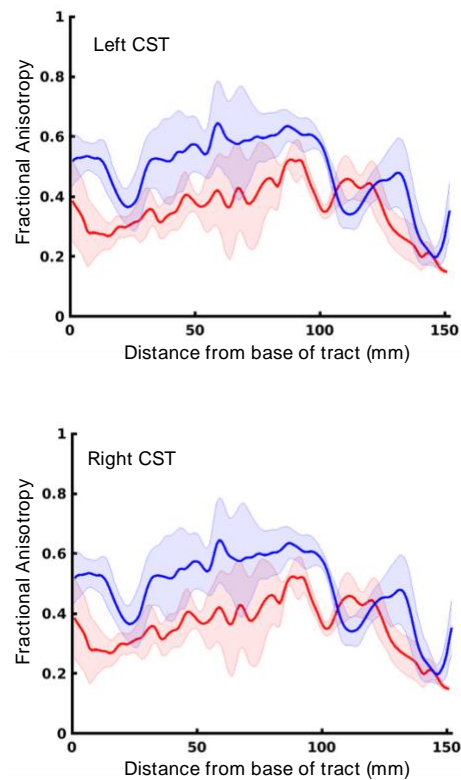
Corticospinal Tracts Derived from Diffusion Tensor Imaging

Diffusion tensor imaging (DTI) demonstrated intact corticospinal tracts arising from typical (left hand) and displaced (right hand) regions of motor task response in PS1 relative to a typical control subject (Figure S5). The control subject had slightly higher fractional anisotropy (FA) values along the left and right corticospinal tracts (CST), displayed as a function of distance (in mm) from the base of the tract in the brainstem (Figure S5C). The FA values averaged across the entire CSTs are: PS1 Left: 0.37; PS1 Right: 0.42; Control Left: 0.50; Control Right: 0.51. However, this effect was not evenly distributed along the tract with greater similarity in FA between PS1 and the control subject closer to the cortical surface (~>100 mm from base of tract).

A) Corticospinal Tract (CST): PS1 *vs.* Control
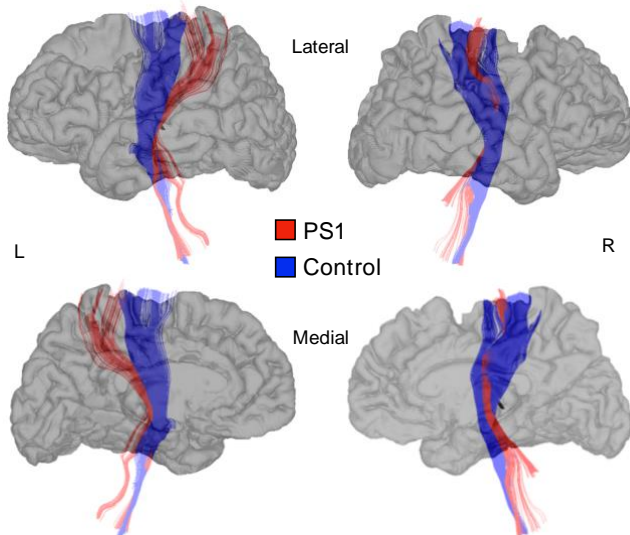
C) FA along Corticospinal Tract: PS1 *vs.* Control

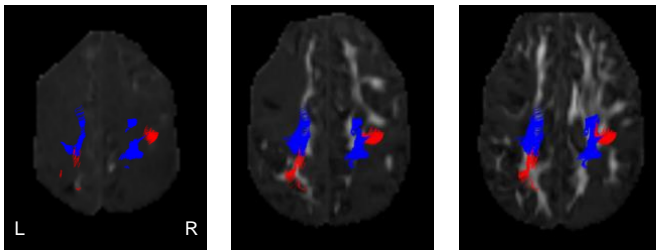B) CST on PS1 Fractional Anisotropy (FA) map

Figure S5. A) Corticospinal tracts (CST) in PS1 compared to a typical control subject. Tracts are visualized inside a glass brain visualization derived from the pial surface of PS1. Tractography was seeded using regions of interest defined by significant task functional MRI (fMRI) responses during left hand and right hand movements. Note that left hand representation follows an overlapping, albeit smaller, path in PS1 relative to the control. The right hand tract in PS1 starts from a displaced position, but ultimately passes through the brainstem appropriately. B) CSTs are visualized over intersecting axial Fractional Anisotropy (FA) maps. C) Mean FA (standard deviation indicated by the shaded region) along the length of the left and right CST for PS1 and control.

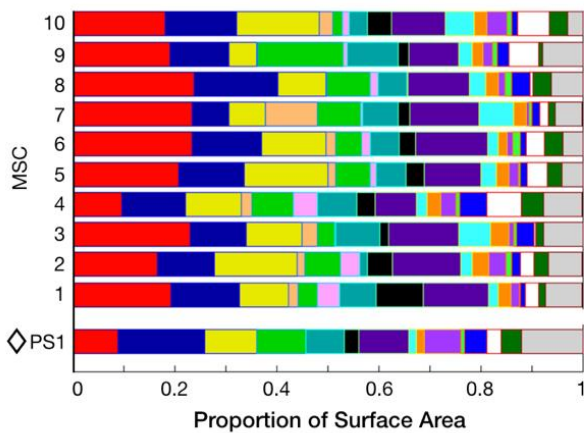## Cortical Functional Network Organization of PS1 Based on RSFC

To understand how PS1's functional brain organization responded to extensive loss of cortical tissue, whole-brain network detection techniques were applied to his RSFC data [60] and compared to a reference dataset [24]. Two major findings emerged from this analysis. First, the overall network spatial pattern, i.e., the adjacency of network regions, appears to have been largely preserved (Figure 1D). Second, resting state

10

functional networks were present in PS1 with mostly typical relative proportions of cortical surface area dedicated to each functional network (Figure S6).
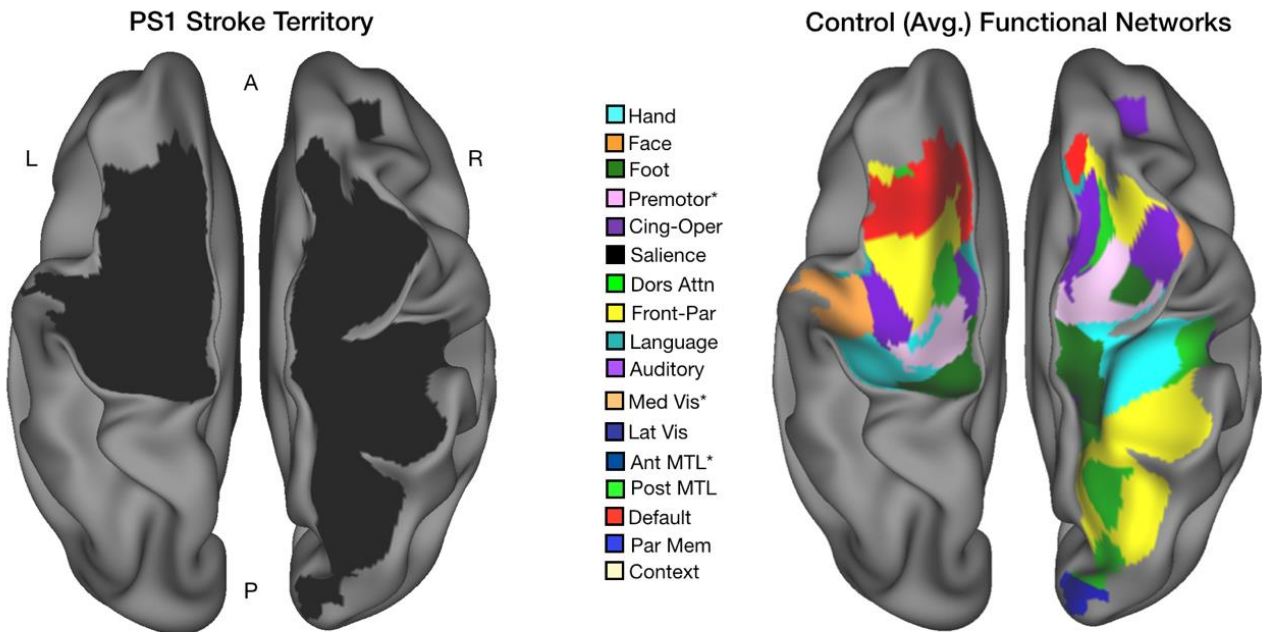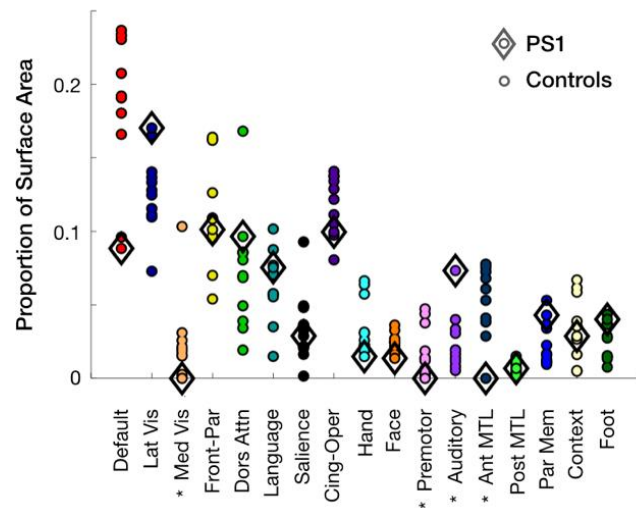

Figure S6. A) Representation of cortical lesion and typical network loss, relative to the average MSC functional network map (dorsal view). B) Proportion of cortex occupied by resting state networks in PS1 relative to typical controls (MSC). Diamond indicates PS1. Almost all of the networks found in typical controls were also identified in PS1. PS1 was missing three networks seen in most typical controls. The first of these networks, labelled the 'premotor' network (pink), localizes to dorsal frontal cortex regions that fall entirely within the region of lost cortical tissue in PS1 bilaterally. The second missing network, labelled the medial visual network (light orange), is not consistently observed across all individuals [24]. Further, its presence has been shown to depend on resting state condition, i.e. it becomes more prominent in eyes closed as compared to eyes open conditions [39]. The third missing network is a small network in the anterior medial temporal lobe (blue-green) that is near susceptibility regions and is of undetermined significance in typical controls. The network identification procedure also labelled in PS1 four small networks that did not have clear correspondence with networks in the MSC dataset. These 'networks' together comprised less than 2% of the cortical surface and fell in typical regions of susceptibility artifact (e.g., occipital pole and anterior temporal cortex). They were therefore ignored in subsequent analyses. C) Alternative representation of proportion of cortex occupied by resting state network in PS1 relative to typical controls (MSC). Diamond indicates PS1. Asterisk indicates networks for which PS1's proportion of surface area is outside the 95% CI of controls.

Given the extent of tissue loss, the relatively typical pattern of functional networks seen in PS1 suggests that functional remapping has occurred. For example, note the functional network arrangement shared between PS1 and controls in lateral parietal and occipital cortex comprising in sequence visual (blue) → dorsal attention (green) → default mode (red) networks (Figure S7). In typical controls, the dorsal attention network (DAN) component of this network motif occupies a large swath of the intraparietal sulcus. In PS1, this region of DAN appears to have shifted to intact lateral occipital cortex, but remains between the visual and default mode networks. Similarly, note on the dorsal lateral frontal cortex, another shared network motif in PS1 and controls comprising fronto-parietal (yellow) → language (teal) → cingulo-opercular (purple) networks. In PS1, this motif has shifted ventrally and anteriorly relative to the lesion. Correlation maps from one network in each motif are shown in Figure S7 to illustrate the underlying RSFC shifts in PS1 relative to controls (Figure S7, arrows).
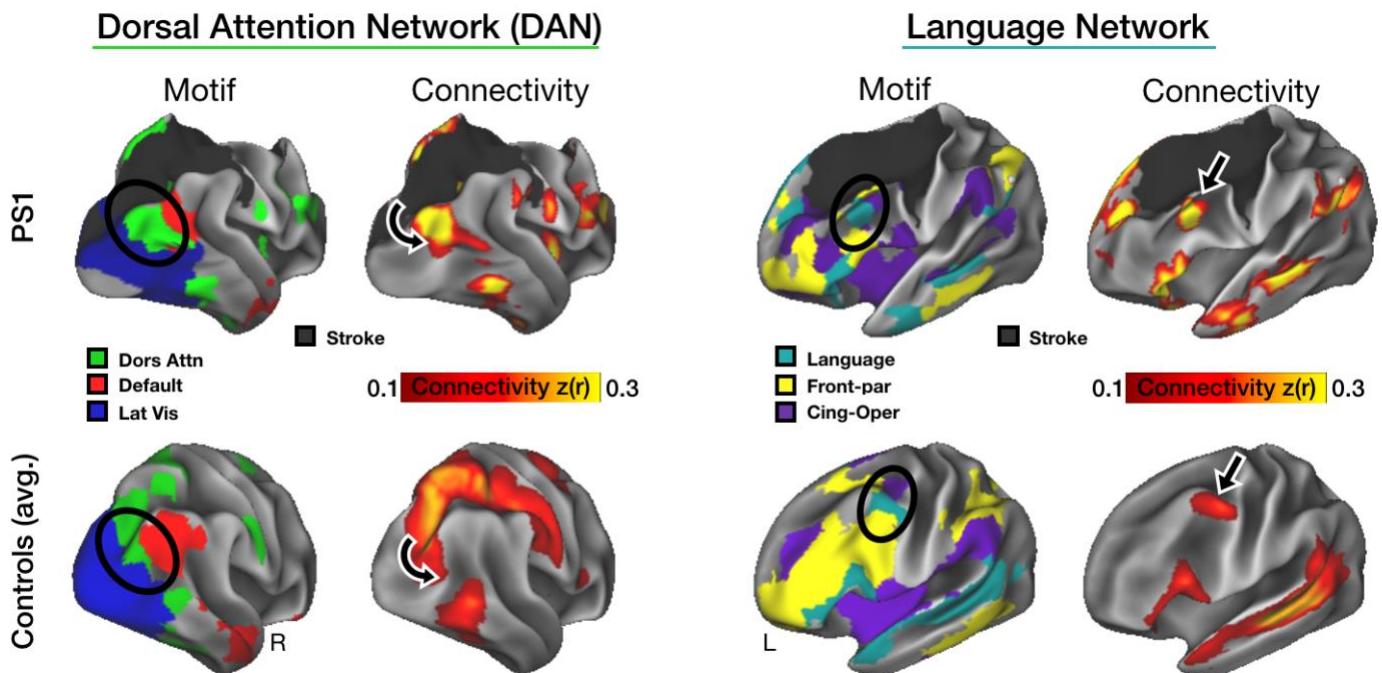

Figure S7. Examples of positional shifts in PS1's resting state functional connectivity (RSFC) with maintained network motifs (black circles). On the left, visual (blue), dorsal attention (green), and default (red) networks shift laterally and ventrally away from the lesion. To illustrate the shift in underlying RSFC, the dorsal attention network correlation maps from the control group and PS1 are shown (black arrows). On the right, the fronto-parietal (yellow), language (teal), and cingulo-opercular (purple) networks shift ventrally and anteriorly away from the lesion. To illustrate the shift in underlying RSFC, the language network correlation maps from the control group and PS1 are shown (black arrows).

Discussion

PS1 is a remarkable individual with typical function despite extensive bilateral cortical injury early in life. We characterized the details of functional plasticity associated with this exceptional compensatory feat using repeated *in vivo* neuroimaging, following newly defined protocols for precision functional mapping (PFM) in individuals [24, 39, 40, 61, 62]. Notable observations derived from this unique dataset are discussed below.

Motor Function Depends on Extent and Localization of Cortical Injury

PS1's left hand motor representation occupies a remarkably small territory of the right central sulcus. Motor task activation was present on islands of cortical tissue otherwise largely disconnected from the cortical sheet. Yet, PS1's left hand motor function was normal, or even supra-normal – he was a pitcher for a competitive youth baseball team. In contrast, the right hand was functionally impaired, despite the motor activity (fMRI) occupying a larger extent of cortical territory. Crucially, the right-hand motor territory was posteriorly displaced to the post-central gyrus following complete loss of the pre-central gyrus. These observations suggest that intact motor function can be supported by a small remnant of the cortico-spinal tract, which may rely on the

continued presence of Betz cells with direct connectivity to anterior horn cells of the spinal cord, whereas projections from the post-central gyrus cannot support typical levels of motor ability. Thus, while significant functional motor remapping is possible, it is likely limited by demand for specific neuronal circuits established prior to the first month of life.

Displaced but Intact Functional Networks Support Typical Function

A characteristic pattern of functional networks has been consistently replicated in typically developed adults based on whole brain RSFC analyses [24, 60]. PS1 provides evidence that the presence of a nearly full complement of functional networks with normal neighbor relations and relative size, albeit remapped due to loss of cerebral cortex, can act as a marker of intact functioning. This result is consistent with the principle that typical cognitive function depends on intact functional connectivity [63]. Importantly, PS1's resting state data suggest that intact brain functioning is less dependent on the exact location and size of regions than might be expected. Following this principle, one might expect to find distorted, but intact, functional networks in the cognitively intact hydrocephalic cases that have previously been noted in the literature [64, 65]. Consistent with this inference, Kliemann and colleagues have found typical RSFC patterns in the intact hemisphere of post-hemispherotomy patients [17]. Yet, a full complement of functional networks does not preclude neuropsychiatric pathology (e.g., RSFC abnormalities in schizophrenia are subtle [66]). Conversely, grossly abnormal resting state activity typically indicates neurologic impairment, e.g., [63].

Patient-specific Precision Mapping Captures Functional Reorganization Following Perinatal Stroke

Cases of relatively preserved cognition in survivors of perinatal stroke have been reported previously [3]. It is believed that this phenomenon reflects functional remapping [3, 12]. Task fMRI has previously demonstrated alternative localization of functional activity in specific functional domains (e.g., language or motor) in cases of cortical injury, e.g., [11, 13]. In contrast, here, we document re-organization across functional systems in an individual. This analysis is enabled by extensive functional imaging of both task (2.28 hrs) and rest (4.75 hrs), which stands in contrast to typical fMRI protocols (5-20 mins per subject).

We cannot directly infer the molecular mechanisms responsible for the observed functional remapping on the basis of fMRI. However, thalamocortical communication is central to the process of cortical organization during development [67, 68]. Thus, we speculate that the extent of PS1's functional remapping reflects the fact that his subcortical structures were entirely spared.

The comparisons between PS1 and the healthy controls are somewhat limited by their difference in age at time of scanning (PS1 = 16 yo, HC = 24-34 yo). Extensively-sampled individual adolescent healthy control datasets are not currently available. However, analyses of the Adolescent Brain Cognitive Development (ABCD) study, a large-scale study (n = 11,874) of resting-state data in 9-10 year olds, have demonstrated that adult network topology is largely present by late childhood [69].

The individual-specific comparison between PS1 and typical controls confirms that largely typical development is possible despite extensive early-life cortical brain injury. In particular, typical motor function can be supported by a remarkably small preserved island of primary motor cortex. On the other hand, remapped function to atypical cortical territory may only partially compensate for lost tissue. More broadly, our results suggest that typical function is supported by intact functional networks. In the context of the prognostic challenges following perinatal stroke, our results raise the possibility that variability in outcome will be reflected in the specific features of individual functional connectomes. Indeed, the success of intact functional remapping may account for the particularly positive outcome observed in PS1.

Acknowledgements

References

1. Raybaud, C., *Destructive lesions of the brain.* Neuroradiology, 1983. **25**(4): p. 265-91.
2. Lehman, L.L. and M.J. Rivkin, *Perinatal arterial ischemic stroke: presentation, risk factors, evaluation, and outcome.* Pediatr Neurol, 2014. **51**(6): p. 760-8.
3. Kirton, A. and G. Deveber, *Life after perinatal stroke.* Stroke, 2013. **44**(11): p. 3265-71.
4. Lee, J., et al., *Predictors of outcome in perinatal arterial stroke: a population-based study.* Ann Neurol, 2005. **58**(2): p. 303-8.
5. Mercuri, E., et al., *Neonatal cerebral infarction and neuromotor outcome at school age.* Pediatrics, 2004. **113**(1 Pt 1): p. 95-100.
6. Sreenan, C., R. Bhargava, and C.M. Robertson, *Cerebral infarction in the term newborn: clinical presentation and long-term outcome.* J Pediatr, 2000. **137**(3): p. 351-5.
7. Studer, M., et al., *Factors affecting cognitive outcome in early pediatric stroke.* Neurology, 2014. **82**(9): p. 784-92.
8. Benton, A.L. and D. Tranel, *Historical notes on reorganization of function and neuroplasticity.*, in *Cerebral Reorganization of Function After Brain Damage.*, H.S. Levin and J. Grafman, Editors. 2000, Oxford University Press: New York. p. 3-23.
9. Grefkes, C. and N.S. Ward, *Cortical reorganization after stroke: how much and how functional?* Neuroscientist, 2014. **20**(1): p. 56-70.
10. Levin, H.S., *Neuroplasticity following non-penetrating traumatic brain injury.* Brain Inj, 2003. **17**(8): p. 665-74.
11. Rehme, A.K., et al., *Activation likelihood estimation meta-analysis of motor-related neural activity after stroke.* Neuroimage, 2012. **59**(3): p. 2771-82.
12. Stiles, J., et al., *Cognitive development following early brain injury: evidence for neural adaptation.* Trends Cogn Sci, 2005. **9**(3): p. 136-43.
13. Fair, D.A., et al., *The functional organization of trial-related activity in lexical processing after early left hemispheric brain lesions: An event-related fMRI study.* Brain Lang, 2010. **114**(2): p. 135-46.
14. Staudt, M., et al., *Two types of ipsilateral reorganization in congenital hemiparesis: a TMS and fMRI study.* Brain, 2002. **125**(Pt 10): p. 2222-37.
15. Ward, N., *Assessment of cortical reorganisation for hand function after stroke.* J Physiol, 2011. **589**(Pt 23): p. 5625-32.
16. Kelly, C. and F.X. Castellanos, *Strengthening connections: functional connectivity and brain plasticity.* Neuropsychol Rev, 2014. **24**(1): p. 63-76.
17. Kliemann, D., et al., *Intrinsic Functional Connectivity of the Brain in Adults with a Single Cerebral Hemisphere.* Cell Rep, 2019. **29**(8): p. 2398-2407 e4.
18. Carter, A.R., G.L. Shulman, and M. Corbetta, *Why use a connectivity-based approach to study stroke and recovery of function?* Neuroimage, 2012. **62**(4): p. 2271-80.
19. Grefkes, C. and G.R. Fink, *Connectivity-based approaches in stroke and recovery of function.* Lancet Neurol, 2014. **13**(2): p. 206-16.
20. Kennard, M.A., *Age and other factors in motor recovery from precentral lesions in monkeys.* Americal Journal of Physiology, 1936. **115**: p. 138 - 146.
21. Newbold, D.J., et al., *Plasticity and Spontaneous Activity Pulses in Disused Human Brain Circuits.* Neuron, 2020. **107**(3): p. 580-589 e6.
22. Max, J.E., et al., *Pediatric stroke: plasticity, vulnerability, and age of lesion onset.* J Neuropsychiatry Clin Neurosci, 2010. **22**(1): p. 30-9.
23. Mosch, S.C., J.E. Max, and D. Tranel, *A matched lesion analysis of childhood versus adult-onset brain injury due to unilateral stroke: another perspective on neural plasticity and recovery of social functioning.* Cogn Behav Neurol, 2005. **18**(1): p. 5-17.
24. Gordon, E.M., et al., *Precision Functional Mapping of Individual Human Brains.* Neuron, 2017. **95**(4): p. 791-807 e7.

25. Kaufman, A.S. and N.L. Kaufman, *Kaufman Brief Intelligence Test.* 2 ed. 2014: Encyclopedia of Special Education.
26. *NIH Toolbox: Cognition Battery.* 2015, Northwestern University and the National Institutes of Health.
27. Achenbach, T.M., & Rescorla, L. A., *Manual for the ASEBA preschool forms & profiles.* 2000, Burlington, VT: University of Vermont, Research Center for Children, Youth, and Families.
28. Kovacs, M., *Children's Depression Inventory.* Pearson Assessments, 2010.
29. Kreutzer, J.S., B. Caplan, and J. DeLuca, *Encyclopedia of clinical neuropsychology.* 2011, New York ; London: Springer.
30. Arnould, C., et al., *ABILHAND-Kids: a measure of manual ability in children with cerebral palsy.* Neurology, 2004. **63**(6): p. 1045-52.
31. Henderson, S.E., D.A. Sugden, and A.L. Barnett, *Movement Assessment Battery for Children - 2 Examiner's Manual.* 2007.
32. Mathiowetz, V., D.M. Wiemer, and S.M. Federman, *Grip and Pinch Strength: Norms for 6- to 19-Year-Olds.* American Journal of Occupational Therapy, 1986. **40**(10): p. 705-711.
33. Skogan, A.H., et al., *Updated developmental norms for fine motor functions as measured by finger tapping speed and the Grooved Pegboard Test.* Dev Neuropsychol, 2018. **43**(7): p. 551-565.
34. Mathiowetz, V., S.M. Federman, and D.M. Wiemer, *Box and Block Test of Manual Dexterity: Norms for 6–19 Year Olds.* Canadian Journal of Occupational Therapy, 1985. **52**(5): p. 241-245.
35. Randall, M., L. Johnson, and D. Reddihough, *The Melbourne Assessment.* Melbourne: Royal Children's Hospital, 1999.
36. Barch, D.M., et al., *Function in the human connectome: task-fMRI and individual differences in behavior.* Neuroimage, 2013. **80**: p. 169-89.
37. Andersson, J.L.R. and S.N. Sotiropoulos, *An integrated approach to correction for off-resonance effects and subject movement in diffusion MR imaging.* Neuroimage, 2016. **125**: p. 1063-1078.
38. Verde, A.R., et al., *UNC-Utah NA-MIC framework for DTI fiber tract analysis.* Front Neuroinform, 2014. **7**: p. 51.
39. Laumann, T.O., et al., *Functional System and Areal Organization of a Highly Sampled Individual Human Brain.* Neuron, 2015. **87**(3): p. 657-70.
40. Marek, S., et al., *Spatial and Temporal Organization of the Individual Human Cerebellum.* Neuron, 2018. **100**(4): p. 977-993 e7.
41. Dale, A.M., B. Fischl, and M.I. Sereno, *Cortical surface-based analysis. I. Segmentation and surface reconstruction.* Neuroimage, 1999. **9**(2): p. 179-94.
42. Fischl, B., M.I. Sereno, and A.M. Dale, *Cortical surface-based analysis. II: Inflation, flattening, and a surface-based coordinate system.* Neuroimage, 1999. **9**(2): p. 195-207.
43. Van Essen, D.C., et al., *Parcellations and hemispheric asymmetries of human cerebral cortex analyzed on surface-based atlases.* Cereb Cortex, 2012. **22**(10): p. 2241-62.
44. Robinson, E.C., et al., *MSM: a new flexible framework for Multimodal Surface Matching.* Neuroimage, 2014. **100**: p. 414-26.
45. Glasser, M.F. and D.C. Van Essen, *Mapping human cortical areas in vivo based on myelin content as revealed by T1- and T2-weighted MRI.* J Neurosci, 2011. **31**(32): p. 11597-616.
46. Talairach, J. and P. Tournoux, *Co-planar stereotaxic atlas of the human brain : 3-dimensional proportional system : an approach to cerebral imaging.* 1988, Stuttgart ; New York: Georg Thieme. 122 p.
47. Smith, S.M., et al., *Advances in functional and structural MR image analysis and implementation as FSL.* Neuroimage, 2004. **23 Suppl 1**: p. S208-19.
48. Miezin, F.M., et al., *Characterizing the hemodynamic response: effects of presentation rate, sampling procedure, and the possibility of ordering brain activity based on relative timing.* Neuroimage, 2000. **11**(6 Pt 1): p. 735-59.
49. Ciric, R., et al., *Benchmarking of participant-level confound regression strategies for the control of motion artifact in studies of functional connectivity.* Neuroimage, 2017. **154**: p. 174-187.
50. Power, J.D., et al., *Methods to detect, characterize, and remove motion artifact in resting state fMRI.* Neuroimage, 2014. **84**: p. 320-41.
51. Fair, D.A., et al., *Correction of respiratory artifacts in MRI head motion estimates.* Neuroimage, 2020. **208**: p. 116400.

52. Gratton, C., et al., *Removal of high frequency contamination from motion estimates in single-band fMRI saves data without biasing functional connectivity.* Neuroimage, 2020. **217**: p. 116866.

53. Power, J.D., et al., *Spurious but systematic correlations in functional connectivity MRI networks arise from subject motion.* Neuroimage, 2012. **59**(3): p. 2142-54.

54. Hallquist, M.N., K. Hwang, and B. Luna, *The nuisance of nuisance regression: spectral misspecification in a common approach to resting-state fMRI preprocessing reintroduces noise and obscures functional connectivity.* Neuroimage, 2013. **82**: p. 208-25.

55. Carp, J., *Optimizing the order of operations for movement scrubbing: Comment on Power et al.* Neuroimage, 2013. **76**: p. 436-8.

56. Behzadi, Y., et al., *A component based noise correction method (CompCor) for BOLD and perfusion based fMRI.* Neuroimage, 2007. **37**(1): p. 90-101.

57. Raut, R.V., et al., *On time delay estimation and sampling error in resting-state fMRI.* Neuroimage, 2019. **194**: p. 211-227.

58. Glasser, M.F., et al., *The minimal preprocessing pipelines for the Human Connectome Project.* Neuroimage, 2013. **80**: p. 105-24.

59. Rosvall, M. and C.T. Bergstrom, *Maps of random walks on complex networks reveal community structure.* Proc Natl Acad Sci U S A, 2008. **105**(4): p. 1118-23.

60. Power, J.D., et al., *Functional network organization of the human brain.* Neuron, 2011. **72**(4): p. 665-78.

61. Greene, D.J., et al., *Integrative and Network-Specific Connectivity of the Basal Ganglia and Thalamus Defined in Individuals.* Neuron, 2020. **105**(4): p. 742-758 e6.

62. Sylvester, C.M., et al., *Individual-specific functional connectivity of the amygdala: A substrate for precision psychiatry.* Proc Natl Acad Sci U S A, 2020. **117**(7): p. 3808-3818.

63. Pizoli, C.E., et al., *Resting-state activity in development and maintenance of normal brain function.* Proc Natl Acad Sci U S A, 2011. **108**(28): p. 11638-43.

64. Feuillet, L., H. Dufour, and J. Pelletier, *Brain of a white-collar worker.* Lancet, 2007. **370**(9583): p. 262.

65. Alvin, M.D. and P.E. Miller, *Compensated hydrocephalus.* Lancet, 2016. **387**(10036): p. 2422.

66. Pearlson, G.D., *Functional MRI Findings in Schizophrenia.*, in *Neuroimaging in Schizophrenia.* , M. Kubicki and M. Shenton, Editors. 2020, Springer, Cham. p. 113 - 124.

67. Martini, F.J., et al., *Impact of thalamocortical input on barrel cortex development.* Neuroscience, 2018. **368**: p. 246-255.

68. O'Leary, D.D., B.L. Schlaggar, and R. Tuttle, *Specification of neocortical areas and thalamocortical connections.* Annu Rev Neurosci, 1994. **17**: p. 419-39.

69. Marek, S., et al., *Identifying reproducible individual differences in childhood functional brain networks: An ABCD study.* Dev Cogn Neurosci, 2019. **40**: p. 100706.

Supplemental Video 1

Video S1. PS1 working in a machine shop in St. Louis, Missouri in the summer of 2011. Note subtle motor deficit in right hand, but otherwise normal movements.